Self-healing and Adhesive Super-soft Materials Derived from Dynamically Cross-linked Bottlebrush Polymer for Flexible Sensors

Erqiang Du[1], Mengke Li[3], Binbin Xu[2], Yingxin Zhang[2], Zibiao Li[4], Xiaohui Yu[2, 4, *]and Xiaoshan Fan[3, *]

[1] School of Automobile and Mechatronics Engineering, Zhoukou Vocational and Technical College, Zhoukou, Henan 466000, China

[2] State Key Laboratory for Modification of Chemical Fibers and Polymer Materials, College of Materials Science and Engineering, Donghua University, Shanghai 201620, P. R. China

[3] Key Laboratory of Green Chemical Media and Reactions Ministry of Education, School of Chemistry and Chemical Engineering, Henan Normal University, Xinxiang 453007, P. R. China

[4] Institute of Sustainability for Chemicals, Energy and Environment (ISCE2), Agency for Science, Technology and Research (A*STAR), 1 Pesek Road, Jurong Island, Singapore 627833, Republic of Singapore

ABSTRACT: Multifunctional bottlebrush polymer super-soft materials are highly desirable for the development of next-generation flexible electronic devices. Herein, we report a facile strategy for the fabrication of bottlebrush polymer super-soft materials integrated with self-healing and adhesive functionalities. These are achieved by the first fabrication of the bottlebrush poly(*n*-butyl acrylate) (P*n*BA) via combining ATRP with ROMP and subsequent

formation of dynamically cross-linked networks via “click” thiol-bromo reaction between Br end groups of P*n*BA side chains and dithiol-containing boronic ester (BDB) crosslinker. Owing to the unique architecture and the reversible boron ester bonds, the unique bottlebrush architecture and fast bond-reforming kinetics of boron ester bonds impart the resultant materials with super-softness with a shear modulus as low as 5 kPa and high self-healing efficiency over 90%. Moreover, owing to the extremely low glass transition temperature of P*n*BA segments, they also display strong adhesiveness to many substrates. The as-prepared strain sensors show an excellent ability to detect a large range of strains from ultralow strain of 0.1% to large strain of 100%. This work has provided a facile and promising approach to the development of multifunctional super-soft materials, which hold great potential as functional sensors for flexible electronics.

KEYWORDS: Bottlebrush Polymer, Super-softness, Self-healing, Adhesiveness, Flexible Sensor

1. INTRODUCTION

In recent years, electronic sensors with flexible and stretchable features have received increasing attention in a broad range of applications such as wearable electronics, electronic skin, soft robotics, implantable electronic devices and human-machine interfacing.[1-3] Tremendous efforts have been directed toward fabricating high-performance electronic sensors with flexibility and stretchability.[4, 5] In spite of rapid advances accomplished, there still are some problems that cause great limitation on their applications and are required to be resolved. In particular, modulus of the polymer matrix applied in most flexible sensors is much higher than that of the human skin, and it is difficult for these sensors to make coincident deformations with the skin for detecting low strain (<1%).[6-8] The strategies of the complex unique structure and the ultra-thin feature have been taken to achieve higher gauge factors (GFs) at low strain in the flexible sensors.[9-11] The obtained sensors with low modulus show good conformal adhesion to the skin and can recognize extremely low strain, however, they usually have lower detection range (<10%) and the ultrathin film and unique structures are easily broken in harsh working conditions.[12, 13] Due to their unique properties, hydrogels have been utilized to fabricate mechanically soft wearable sensors.[14-17] However, these systems confront the problem of unstability since the softness of the materials will decrease with the solvent gradually evaporating.[18, 19] Therefore, it is yet challenging to develop mechanically stable super-soft materials for the fabrication of high-performance soft electronic.

Bottlebrush polymers with densely grafted side chains have an extended backbone resulting from the repulsion between the side chains.[20-27] As compared with their linear analogs, one unique attribute of bottlebrush polymers is their significantly suppressed chain entanglements

in the networks.[28-33] Thus, lightly cross-linking bottlebrush polymers provides a promising avenue for achieving the solvent-free super-soft materials.[34, 35] Progress has been made in the development of bottlebrush polymer based high-performance materials, especially those with self-healing capability, which can repeatedly repair mechanical damages and restore their functionality, resulting in enhanced durability of the materials with prolonged service lifetime.[36-39] However, the preparation process of dynamically cross-linked bottlebrush polymers mostly involves tedious functional end groups transformation of side chains and/or synthesis of small molecular crosslinkers.[21, 40] Meanwhile, the resultant materials usually fulfill the self-healing behavior under elevated temperature, thereby limiting their applications in practice.[41, 42] It should be further noted that the bioelectronic devices need to have direct contact with human skin for effective signal transduction.[43-46] To the best of our knowledge, few of literature bottlebrush polymer based super-soft materials possess adhesive capability and adhesive tapes or binding bandages are needed to fix the fabricated wearable sensors onto human skin.[47, 48] Apart from consideration of simplifying the operation process, it is also difficult for them to perfectly detect micro-strains and feeble physiological signals.[6] Therefore, it still remains a challenge to integrate the combination of excellent self-healing capability and adhesiveness into one bottlebrush polymer based super-soft material, which is critical for the development of next-generation flexible electronic devices with high-quality and stable electrophysiological recordings.

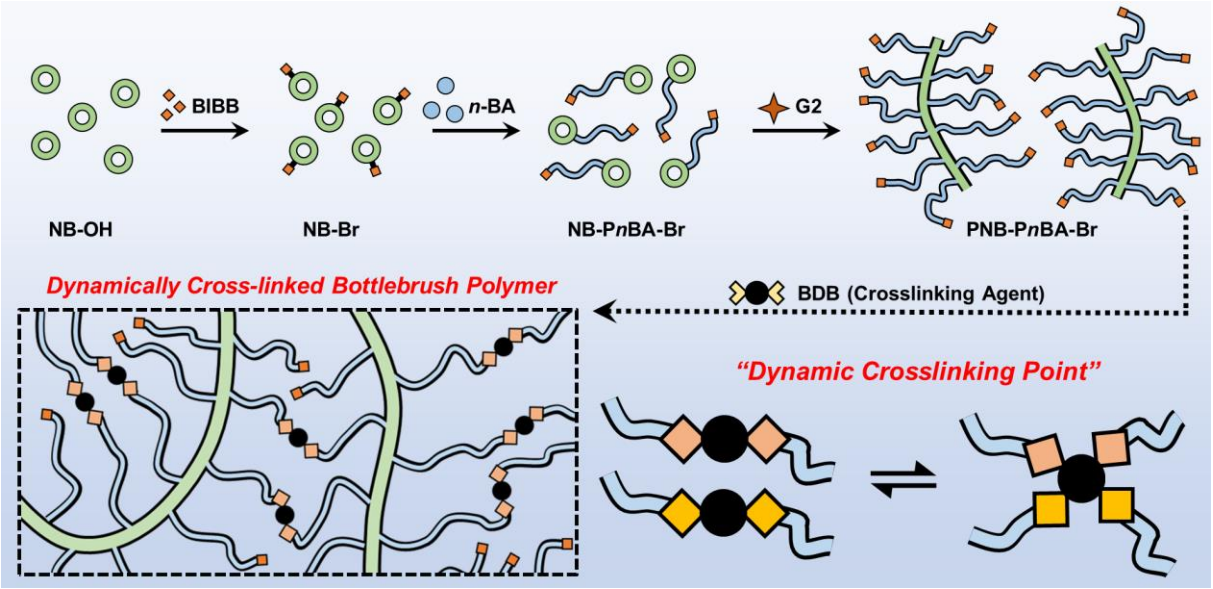

Figure 1. Design of the P*n*BA bottlebrush polymer material with dynamic crosslinking points, aiming to achieve enhanced self-healing capability, and remarkable super-soft mechanical properties.

Here, we proposed a facile yet simple strategy that combines the benefits of molecular architecture and dynamic bonds to access dynamically cross-linked bottlebrush polymer super-soft materials integrated with self-healing and adhesive properties. As depicted in **Figure 1**, this is achieved by the combination of atom transfer radical polymerization (ATRP), ring-opening metathesis polymerization (ROMP) and "click" thiol-bromo coupling reaction. In comparison with reported strategies for fabricating high-performance bottlebrush polymer based materials, the strategy demonstrated here have several advantages. First, Br end-groups at the P*n*BA side chains derived from ATRP can directly react with thiol-containing crosslinker, thus avoiding tedious end-group transformation. Second, "click" thiol-bromo reaction for cross-linking the bottlebrush polymer precursor can be rapidly completed under ambient conditions, which is favorable to simplify the operation process. Last, due to the extremely low glass transition temperature of P*n*BA, the obtained materials exhibit excellent adhesiveness toward many contacted substrates, which facilitates the stability of signal detection. As a strain sensor,

the P*n*BA bottlebrush polymer elastomers shows high sensing performance in a broad range of detection (0.5% ~100%). Several unique attributes mentioned above make the P*n*BA bottlebrush polymer elastomer a promising candidate for applications in soft electronic devices.

2. RESULTS AND DISCUSSION

2.1. Preparation of the Bottlebrush Polymeric Material

The bottlebrush polymeric material was obtained by crosslinking the macromolecular bottlebrush polymer with the dithiol-containing boronic ester crosslinker via the thiol-bromo "click" reaction.[49] At first, the bottlebrush polymer was synthesized by the "grafting through" strategy as depicted in **Figure 2A**.[29] The initiator monomer bromine functionalized norbornene (NB-Br) was obtained by the reaction of 2-bromo-isobutyryl-bromide (BIBB) with 5-norbornene-2-methanol (NB-OH). ^{1}H nuclear magnetic resonance (^{1}H NMR) spectra confirms the chemical structure of NB-Br (**Figure 2B**), in which the characteristic peaks assigned to alkene protons at 5.90~6.21 ppm of NB moiety and methyl protons (-OCOC(CH_3)Br) at 1.88 ppm of BIBB segment can be observed clearly. Afterwards, the obtained NB-Br initiated the polymerization of *n*-butylacrylate (*n*-BA) to generate the norbornene-terminated macromonomers (NB-P*n*BA-Br) via ATRP.[50, 51] The successful synthesis of the product of NB-P*n*BA-Br was confirmed by H^{1}-NMR and the size exclusion chromatography (SEC) techniques. The characteristic peaks attributed to the protons of *n*BA repeating unit can be seen clearly in **Figure 2B** and the SEC trace is a monomodal peak as shown in **Figure 2C**. Integration of alkene protons of the end NB moiety and the methylene protons neighboring to the ester group in P*n*BA segments was used to determine the degree of polymerization and the value is about

20. Subsequent polymerization of P*n*BA via "grafting-through" ROMP provided the bottlebrush polymer precursor NB-P*n*BA-Br.[21, 52] As shown in **Figure 2B** and **2C**, the complete disappearance of the characteristic signals of alkene protons of NB terminal groups and SEC trace obviously shifting toward the higher molecular region as compared with NB-P*n*BA-Br precursor indicate the successful fabrication of PNB-P*n*BA-Br.

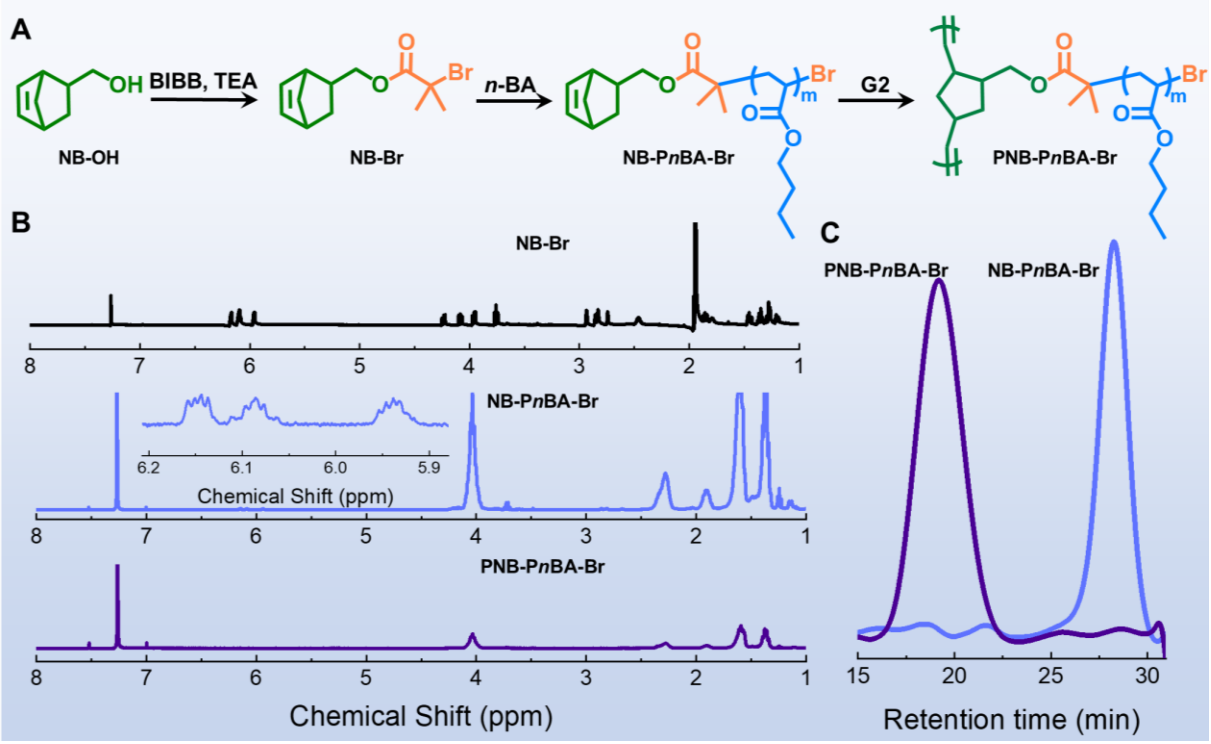

Figure 2. Synthesis and characterization of the bottlebrush norbornene-functionalized macromonomer. (A) Schematic illustration of synthesis of the initiator NB-Br, macromolecular monomer NB-P*n*BA-Br, and bottlebrush polymer PNB-P*n*BA-Br; **(B)** ^{1}H NMR spectra of NB-Br, NB-P*n*BA-Br, and PNB-P*n*BA-Br; **(C)** SEC curves of NB-P*n*BA-Br, and PNB-P*n*BA-Br.

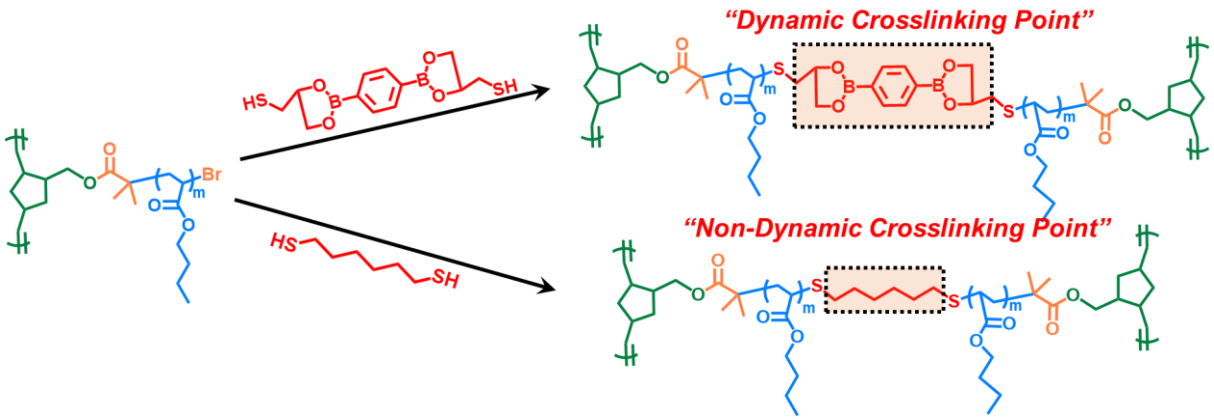

Scheme 1. Schematic illustration of the synthetic route of the Brush-DM and Brush-NM featuring with the dynamic crosslinking point and non-dynamic crosslinking point, respectively.

As followed, the dithiol-containing boronic ester crosslinker (BDB), was introduced into the macromolecular precursors to form the crosslinked polymer network (as illustrated in **Scheme 1**, and **Scheme S1**). As shown in the FT-IR spectra, the peaks located at 2563 and 1219 cm^{-1} could be assigned to the stretching vibrations attributed to the thiol group (-SH) and boron-oxygen bond (B-O), respectively, confirming the successful synthesis of BDB (**Figure S1**).[53, 54] Additionally, the chemical structure of BDB was further substantiated by its ^{1}H NMR spectrum (**Figure S2**). Specifically, the thiol group on BDB could undergo the thiol-bromo "click" reaction with the terminal bromine on the side chains of the bottlebrush polymers, leading to the formation of the dynamic crosslinking point.[55] Thanks to the well-designed architecture, we successfully synthesized the dynamically crosslinked bottlebrush polymer super-soft material, referred to as Brush-DM. Additionally, the non-dynamically crosslinked bottlebrush polymer material, crosslinked using the traditional dithiol molecule, was named Brush-NM (**Scheme 1**). Furthermore, we prepared the linear nondynamic elastomer (Linear-NM) following established procedures (as illustrated in **Scheme S2**).[56]

Brush-DM demonstrates good conductivity (4.1×10^{-3} S m^{-1}) due to the incorporation of lithium bis(trifluoromethane sulfonimide) (LiTFSI), which could transport through the polymer chains.[56, 57] Furthermore, due to its solvent-free composition, Brush-DM stood out for its exceptional environmental stability when exposed to ambient air conditions. As shown in **Figure S3**, the weight of Brush-DM exhibited no discernible signs of weight loss during the storage at various temperatures (25, 50, and 100 ℃) for more than 60 hours. Besides, the conductivity of Brush-DM was also stable (**Figure S4**). This excellent environmental stability underscored its suitability for a wide array of applications in challenging environmental conditions.[8, 19]

2.2. Characterization of Network Structure and Mechanical Performance

It becomes evidently clear that all the samples maintain the rubber-like state at room temperature (25 ℃), a fact that has been confirmed through the rheological amplitude sweeping test.[58] As depicted in **Figure 3A**, the storage modulus (G') of all these samples significantly are higher than their loss modulus (G'') in the plateau region, where sweeping amplitude remains below 50%. To assess the crosslinking densities, we quantified the normalized residual thickness (NRT) of the bottlebrush polymeric materials following the reported paper.[21, 59] A higher NRT indicates a denser polymer network, with an NRT of 100% signifying complete crosslinking. The efficient thiol-bromo "click" reaction facilitated the achievement of high NRT values for both Brush-NM and Brush-DM, at 93.6% and 91.2%, respectively, confirming

the successful formation of covalently crosslinked networks. This remarkable observation underscores the inherent robustness and structural integrity of these materials.

It's worth noting that human skin possesses a modulus substantially lower than that of typical polymeric materials. As a consequence, traditional flexible sensors designed with a focus on mechanical strength face a formidable challenge when it comes to achieving precise deformations in tandem with the substrates they are meant to detect, especially at micro-strain levels. The unfortunate outcome of this challenge is a notable compromise in sensing sensitivity. Therefore, it was imperative to incorporate super-softness to enhance sensing sensitivity and achieve lower detection limits in flexible sensors. In this study, benefiting from the intrinsic bottlebrush structure, the two types of bottlebrush polymer materials (Brush-NM and Brush-DM) both exhibited remarkable softness, characterized by a lower plateau modulus (G_p) of approximately ~8×10^3 Pa and ~5×10^3 Pa, respectively, lower by an order of magnitude compared to Linear-NM (~5×10^4 Pa). To gain insights into the network structure of the samples, we conducted frequency sweeping measurements at a low shearing amplitude of 5%. As shown in **Figure 3B**, G' was consistently higher than G'' within the entire angular frequency range (1 - 100 rad s^{-1}), highlighting the excellent frequency tolerance of the prepared materials.

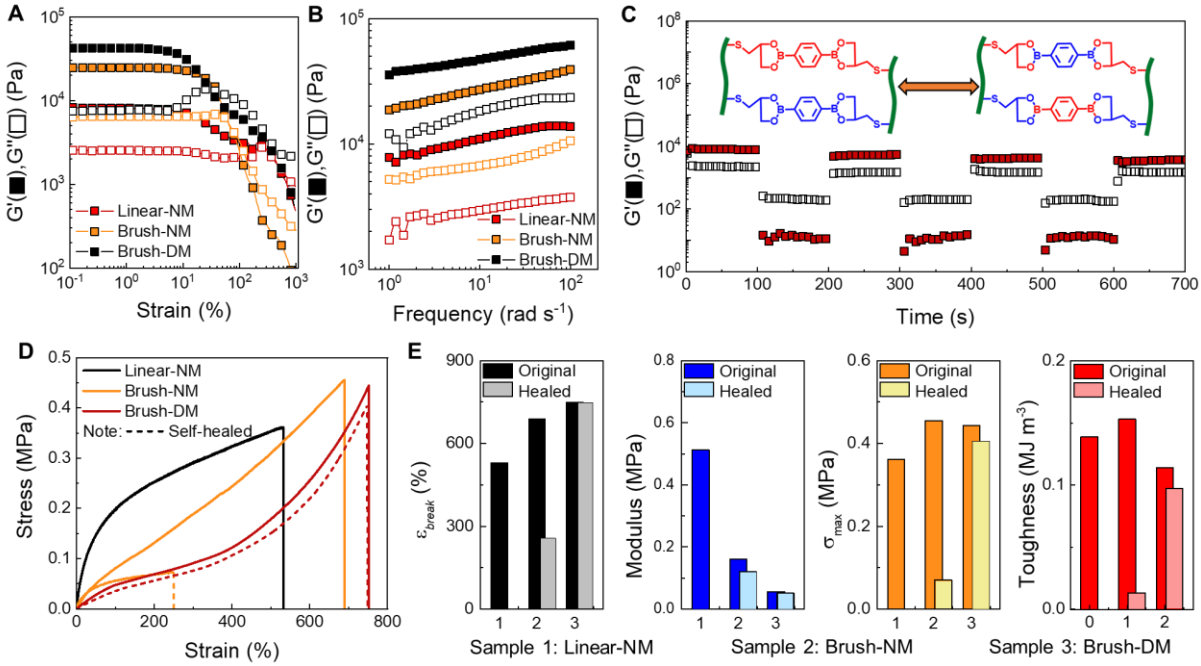

Figure 3. **Network structure and mechanical performance of the prepared materials. (A)** Rheological amplitude sweeping measurement of Linear-NM, Brush-NM and Brush-DM; **(B)** Rheological frequency sweeping measurement of the prepared materials; **(C)** Alternating step strain sweeping measurement of Brush-DM, with an inset schematic illustrating the rearrangement mechanism of the dynamic crosslinked network; **(D)** Tensile curves of the Linear-NM, Brush-NM, and Brush-DM; **(E)** Summary of the mechanical properties (including the elongation at break, Young's Modulus, maximum stress, and toughness) of the above samples.

Notably, Brush-DM stands out as the softer material compared to Brush-NM, thanks to its internal dynamic crosslinking points. **Figure 3A** illustrates that Brush-DM exhibits exceptional softness and deformation tolerance, characterized by the lower G_p and higher transition amplitude of ~451%. Besides, the boronate ester bonds, resulting from the condensation of boronic acids with diols, are durable and stable dynamic covalent bonds capable of reversible rearrangement through hydrolysis/reformation (as illustrated in the inset of **Figure 3C**).[53] Recent studies by Leibler et al. and Guan et al. have demonstrated the ability of boronic ester bonds to undergo associative exchange reactions, facilitating the reorganization of network

topology within bulk polymers, even in solvent-free conditions.[60, 61] This unique property has found successful applications in diverse fields, including the development of self-healing materials and flexible sensors. Leveraging this dynamic characteristic, Brush-DM exhibits remarkable self-healing capability, as evidenced by the alternating step strain sweeping measurement depicted in **Figure 3C**. Under a low shearing strain of 0.5%, Brush-DM remains stably in the rubber-like state for an extended period of 2 minutes. However, at the shearing strain of 500%, the crosslinked network ruptures, resulting in a significant drop of G'. Fortunately, upon reverting the shearing strain back to 0.5%, Brush-DM recovers its rubber-like state with G' exceeding G'' and maintaining a similar value to the initial state. Conversely, Brush-NM exhibited a low self-healing efficiency, as its modulus experienced a significant decrease after cyclic testing (**Figure S5**). The dynamic behavior of the materials could also be observed in the relaxation experiments, as shown in **Figure S6**.[62] The samples were rapidly deformed to a rheological amplitude of 10% and allowed to relax for 10^3 seconds. Compared with the Linear-NE, both bottlebrush polymeric materials demonstrated notable stress relaxation behaviors, due to their intrinsic topological structure. The relaxation curves also provided valuable information on characteristic relaxation times, τ^*, which were determined as the time when $G(t)/G(t_0)$ reached e^{-1}, which is a fundamental concept in rheology and materials science[63, 64]. A longer τ^* indicates a higher cross-linking strength within the polymer network, and vice versa. It could be clearly seen that the τ^* of Brush-DM (~4 s) was much lower than that of the Brush-NM (~10 s) and Linear-NM (~20 s). These remarkable softness, dynamic characteristic and flexibility displayed by Brush-DM hold significant promise for advancing epidemic sensors.

Benefiting from the well-designed network structure, Brush-DM exhibits a comprehensive range of exceptional mechanical properties, making it a highly promising material for sensing application. Its high stretchability and intrinsic elastomeric behavior are evident from the stress-strain curve, which shows no yielding phenomenon during the stretching process, indicating its ability to withstand large deformations while maintaining its elasticity (**Figure 3D**). Even though Brush-DM exhibits a slight decrease in maximum stress (σ_{max}) compared to Brush-NM, it has an increased elongation at break (ε_{break}) (as summarized in **Figure 3E**). Furthermore, Brush-DM demonstrates an impressively softness with a low Young's Modulus, only 0.056 MPa, which is approximately one-tenth of that of Linear-NM (0.512 MPa), showcasing its exceptional super softness and flexibility. This remarkable softness can be attributed to the unique highly branched structure of the bottlebrush polymer, which allows Brush-DM to deform and adapt to various mechanical demands with ease, ensuring both comfort and protection. Additionally, the incorporation of exchangeable crosslinking points endows Brush-DM with efficient self-healing capability, as observed in the stress-strain curves where the self-healed Brush-DM closely aligns with its original curve, indicating its ability to autonomously repair and restore its mechanical properties (**Figure 3D**). The self-healed Brush-DM exhibits significant recovery in terms of elongation at break, Young's Modulus, maximum stress, and toughness, reaching 99.5% (747%), 91.1% (0.051 MPa), 91.2% (0.405 kPa), and 85.1% (0.097 MJ m^{-3}) of the values of the original sample, respectively, demonstrating its exceptional self-healing capability (**Figure 3E**). In contrast, the self-healing efficiency of Brush-NM is exceedingly low for comparison.

To gain insights into the energy dissipation mechanism and mechanical elasticity of Brush-DM, tensile cyclic measurements were also conducted (**Figure S7**). At the maximum loading strain of 100%, the loading-unloading stress-strain curves showed minimal hysteresis with an η of 0.43, indicating efficient energy dissipation.[8] Moreover, throughout subsequent cycles, the values of σ_{max} and η remained stable at 89.9% and 89.3%, respectively, compared to the first cycle, demonstrating the exceptional usage stability of Brush-DM (as summarized in **Figure S8**).

2.3. Self-Adhesive Performance

Furthermore, Brush-DM exhibited a distinct and highly advantageous self-adhesive performance, which plays a pivotal role in enhancing robust interfacial bonding between the material and various substrates, including glass, rubber, and steel. As shown in **Figure 4A**, Brush-DM could be adhered onto various substrates and initiate the lifting of the corresponding objects, demonstrating its excellent interfacial toughness. The outstanding adhesive property of our material is a result of synergistic effects stemming from the well-designed bottlebrush structure and various physical interactions. Above all, the remarkable flexibility endowed by the unique bottlebrush structure enables Brush-DM to conform adeptly to the irregularities and contours of diverse substrates, thereby maximizing the contact area and enhancing adhesion[65, 66]. In addition to this, the strong self-adhesiveness of Brush-DM can be attributed to several possible physical interactions, which including hydrogen bonding with components like -OH, -NH_2, -CO, N, and O groups, metal coordination with metal ions present on solid surfaces, and van der Waals forces[43, 67, 68]. Besides, P*n*BA copolymers and graft copolymers have been

favored in adhesive applications due to their low modulus and glass-transition temperature (Tg)[69].

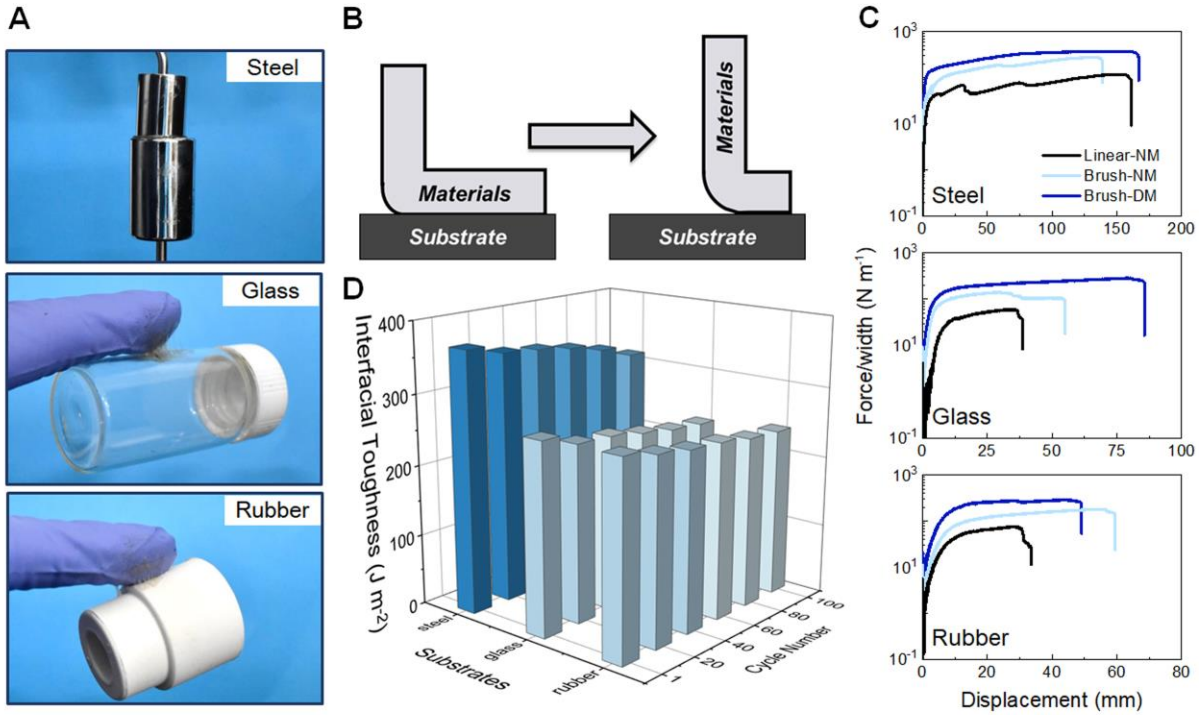

Figure 4. Self-Adhesive performance of the bottlebrush polymeric materials. (A) Photographs of Brush-DM adhered on various substrates, including steel, glass, and rubber; **(B)** Schematic of the 90° peel-off adhesive test of the prepared materials on different substrates; **(C)** Adhesive strength-displacement curves of the different samples on different substrates; **(D)** Cyclic stability of the interfacial toughness of Brush-DM in the cyclic adhere-on/peel-off test.

To quantitatively evaluate their adhesion properties, specifically adhesive strength and interfacial toughness, we conducted a 90° peel-off adhesive test, following the reported works (as shown in **Figure 4B**).[70] As shown in **Figure 4C**, Brush-DM clearly outperformed its counterparts, exhibiting the highest adhesive strength in all the tested substrates. Among them, it achieves a remarkable adhesive strength of 367 N m^{-1} when adhered to glass. As Brush-DM was adhered on steel and rubber, the adhesive strength was 285 N m^{-1}, and 289 N m^{-1},

respectively. Additionally, by integrating the adhesive curves, we derived the interfacial toughness of the material at the aforementioned substrates. This analysis offers further insights into the interfacial strength of the interaction between the material and the tested substrates. As summarized, Brush-DM demonstrated the highest interfacial toughness among the tested materials, achieving values of 273.5 J m^{-2}, 269.2 J m^{-2}, and 368.1 J m^{-2} when adhered to rubber, glass, and steel, respectively, which was much higher than various reported materials (as summarized in **Table S1**). Moreover, to assess the adhesive anti-fatigue performance, 100 cycles adhere-on/peel-off test were performed. The results, illustrated in **Figure 4D**, demonstrated the good stability of interfacial toughness throughout the cyclic test, emphasizing the exceptional anti-fatigue performance of Brush-DM's adhesive capability.

2.4. Mechanoelectronic response and sensing performance

With these above exceptional dynamic mechanical performance, environmental stability, efficient self-healing capability, and good self-adhesive performance, Brush-DM exhibited tremendous potential as an ideal material for engineering flexible sensing devices. As a proof of concept, Brush-DE was successfully utilized in fabricating a conductor for flexible strain sensors, as an initial demonstration of its potential applications. Notably, the sensor did not rely on conductive fillers to create a conductive network, but instead utilize the shape changes of Brush-DE to achieve sensing, resulting in good sensing linearity. The resistance-strain curve demonstrated the sensor's linear response behavior across a wide strain range of up to 100%, showcasing its exceptional sensing sensitivity with a high gauge factor (GF) of 0.997 (**Figure**

5A). As compared, the sensing performance of the strain sensors based on the linear control (Linear-NM) was fabricated and subjected to further testing. As depicted in **Figure S9,** while the resistance-strain curve of the Linear-NM-based sensor exhibited a high degree of linearity, it is noteworthy that its GF was significantly lower, measuring at 0.441, than that of Brush-DM-based sensor. This observation could be attributed to the linear polymer structure, which tends to limit the migration of ions within the network.

Leveraging the remarkable self-healing capability of Brush-DM, the corresponding flexible sensor underwent a loading-unloading process under 100% strain after different healing times. **Figure 5A** illustrated the resistance-strain curves of the sensor at different self-healing times, showing substantial overlap with its original state. Additionally, the GF of the sensor remains consistently stable across various healing times (first = 0.992, second = 0.993, third = 0.994, fourth = 0.992, fifth = 0.993) compared to the original sensor. On the other hand, it's important to highlight that Linear-NM lacks self-healing capabilities, which adversely affects its long-term usage stability. As the Linear-NM-based sensor undergo a cutting-recontacting process, the treated Linear-NM-based sensor lost its sensing capability.

Moreover, the exceptional high elasticity of the material was a key factor in ensuring the Brush-DM-based flexible sensor maintaind excellent cyclic stability even during repeated loading-unloading cycles. The Brush-DM-based sensor consistently maintained remarkable cyclic stability across a wide range of maximum strains (25%, 50%, 75%, and 100%), as evident from the stable electronic patterns depicted in **Figure 5B**. To comprehensively evaluate the sensor's performance, the strain sensing capability was further investigated under different stretching rates, allowing for an assessment of its frequency tolerance. Notably, the results presented in

Figure 5C revealed low fluctuations in the relative resistances at varying loading rates of 30, 50, and 70 mm min^{-1}, confirming the sensor's reliable and stable performance across a wide range of strain rates. To address the cyclic stability of the Brush-DM-based sensor, 100 cyclic uninterrupted loading-unloading tests at the maximum strain of 100% was conducted. As shown in **Figure S10**, it could be observed that there was no significant shift of the baseline of the electronic patterns. The sensor maintained its ability to detect and record strain accurately throughout the extended testing period. Moreover, we investigated the environmental tolerance of the Brush-DM-based flexible sensor under harsh external conditions (90% RH at 50 °C). As illustrated in **Figure S11**, the resistance signal patterns of the sensor after the treatment exhibited a high degree of consistency with the electronic curve of the untreated sensor, providing clear evidence of the remarkable environmental stability of the Brush-DM-based flexible sensor. These remarkable findings highlighted the robust nature and versatility of the Brush-DM-based flexible sensor, positioning it as a promising candidate for diverse dynamic applications with stringent performance requirements.

Considering the diverse range of deformations that occur on the skin, strain sensors need to be capable of detecting both low and high strains. In this study, the Brush-DM-based strain sensor was subjected to ultralow strains of 0.1% to assess its sensing performance in these challenging conditions. Remarkably, the sensor exhibited exceptional sensitivity even at such minuscule deformations, including strains of 0.5%, 1.0%, 1.5%, and 2.0%. This sensitive detection was depicted in **Figure 5D**, where the sensor could accurately capture and measure the ultralow deformations. Furthermore, the electronic pattern displayed distinct periodic changes during

the stepwise loading-unloading process, as illustrated in **Figure 5E**. The sensor's response showed clear and consistent increases and decreases from the original state to a strain of ±0.1%, while maintaining stability under certain strains. This finding indicated that the Brush-DM-based sensor not only detects 0.1% strain but also effectively distinguishes a 0.1% strain difference, making it highly precise in strain measurement. Additionally, the Brush-DM's exceptional conductivity played a crucial role in the sensor's performance. The Brush-DM-based flexible sensors exhibited a remarkably rapid response time of only 140 ms during the stretching-recovering process (**Figure 5E**). This rapid response time highlighted the sensor's ability to capture real-time changes in strain with exceptional speed and accuracy. Based on these remarkable results, we could confidently infer that the Brush-DM-based strain sensor holds significant potential for detecting micro strains on the epidermis. Its ability to sensitively detect ultralow strains and provide precise strain measurements opens up new possibilities in various fields that require precise and accurate strain monitoring.

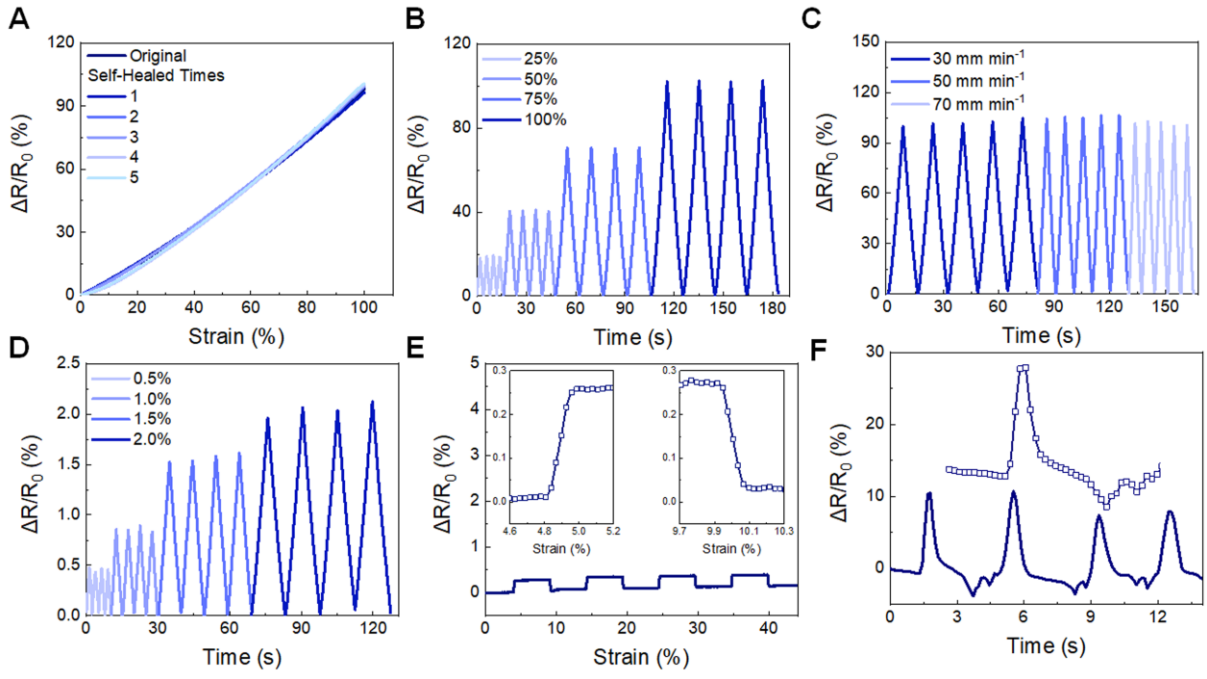

Figure 5. Practical application performance of the Brush-DM-based flexible sensor. (A) Relative resistance ($\Delta R/R_0$) variations of the sensors in different self-healing process with 100% maximum strain; **(B)** Variations in resistance patterns of the sensors under various maximum strains during cyclic testing (25, 50, 75, and 100%); **(C)** Resistance changes relative to strain at 100% under different loading-unloading rates.; **(D)** Electronic patterns of the Brush-DM-based flexible sensor during the loading-unloading tests in different micro-strains of 0.5, 1.0, 1.5, and 2.0%; **(E)** The sensor's electronic patterns in the stepwised cyclic test; **(F)** The changes of the electronic signals of the sensor during wrist bending movements.

In order to evaluate the practical applicability of the sensor, it was utilized on a movable puppet to monitor a range of movements, effectively simulating human behavior. The resulting electronic patterns provided clear distinction between finger and wrist bending activities of the puppet hand. As shown in **Figure S12**, the electronic pattern of the sensor during the bending of the finger was stable and repeatable. Moreover, the wrist movement could be divided into three distinct stages: the initial state, backward, and forward motion (**Figure 5F)**. These stages were precisely mirrored in the electronic patterns, with the initial stage serving as the reference signal platform and the subsequent peaks corresponding to the subsequent motion steps. Throughout these practical applications, the sensor demonstrated exceptional repeatability, maintaining stable signal patterns characterized by consistent signal intensity and a smooth baseline. These results substantiated the sensor's potential for real-time human motion sensing applications.

3. CONCLUSION

In summary, we have developed a facile and promising strategy for the fabrication of multifunctional super-soft materials. This involves the first synthesis of the macromonomer NB-P*n*BA-Br via ATRP, subsequent preparation of the bottlebrush P*n*BA via ROMP and last

cross-linking of the precursor through “click” thiol-bromo reaction between Br end groups and thiol-containing crosslinker BDB. The resulting materials displayed the combined good properties of super-softness, self-healing and adhesiveness. Owing to the characteristics of super-softness and adhesiveness, the further fabricated strain sensors could adhere well with the contacted substrates. Hence, micro stain as low as 0.1% can be perfectly perceived and the high stain (up to 100%) can also be detected due to the excellent stretchability. In addition, the strain sensor exhibited excellent self-healing capability to overcome accidental mechanical damages upon scratch or rupture. We anticipate this type of dynamic supersoft elastomers will find their use in applications for next-generation sensors, which benefit from the combined desirable properties mentioned above.

4. EXPERIMENTAL METHODS

4.1. Materials. The 5-norbornene-2-methanol (NB-OH), 2-bromo-isobutyryl-bromide (BIBB), triethylamine (TEA), *n*-butylacrylate (*n*-BA), N,N,N’,N’,N’’-pentamethyl-diethylenetriamine (PMDETA), copper (I) bromide (CuBr), Grubbs catalyst 2nd (G_2), 1-thioglycerol, 1,4-phenylenediboronic acid, sodium bicarbonate ($NaHCO_3$), anhydrous magnesium sulfate ($MgSO_4$), 2,2-diethoxyacetophenone (DEAP), lithium bis(trifluoromethane sulfonimide) (LiTFSI), 1,6-hexanedithiol and alumina (Al_2O_3) were all purchased from Shanghai Aladdin Biochemical Technology Co., Ltd. Dithiol-containing boronic ester crosslinker (BDB) was synthesized following the reported paper (See details in **Supporting Information**).[54] Acetone, diethyl ether and tetrahydrofuran (THF) were purchased from Sinopharm Chemical Reagent Co. Ltd. Notably, all the solvents were dried by the solvent purification system. Other chemicals

were used without further purification.

4.2. Synthesis of the initiator monomer of NB-Br. In a Schlenk flask, NB-OH (1.24 g, 10.0 mmol), BIBB (3.43 g, 15.0 mmol), and TEA (1.51 g, 15.0 mmol) were dissolved into 50 mL of THF. The resulting mixture was continuously purged with nitrogen for 30 minutes to remove dissolved oxygen. Subsequently, the reaction was stirred for 12 hours in an ice-water bath. Afterward, the mixture was diluted with THF, filtered to remove the white precipitate, and evaporated to dryness under vacuum. The residue obtained after rotary evaporation was dissolved in diethyl ether, and then sequentially washed with deionized water (3×) and saturated $NaHCO_3$ solution (3×). The ethereal phase was collected, dried with $MgSO_4$, and filtered using a Büchner funnel. Finally, the organic phase was concentrated using a rotary evaporator under reduced pressure to obtain the slightly yellow transparent oily final product, the macroinitiator NB-Br. ^{1}H NMR ($CDCl_3$, δ, ppm): 6.16-5.95 (m, 2H, C***H***=C***H***), 4.02 (m, 2H, C***H₂***OCO), 2.93-1.20 (m, 7H, norbornene-7***H***), 1.94 (s, 2H, OCOC***H₂***), 1.93 (s, 6H, C***H₃***).

4.3. Synthesis of the macromonomer of NB-P*n*BA-Br. The macromonomer norbornene-terminated poly(*n*-butylacrylate) (NB-P*n*BA-Br) was synthesized by atom transfer radical polymerization (ATRP) method.[50, 51] Briefly, under nitrogen atmosphere, *n*-BA (4.77 g, 37.2 mmol), PMDETA (0.21 g, 1.2 mmol) and macroinitiator NB-Br (0.14 g, 0.51 mmol) were dissolved into 18 mL acetone in a Schlenk flask. Afterwards, CuBr (0.032 g, 0.22 mmol) was added into the above solution. Following a 4-hour reaction, the solution was diluted with THF and the catalyst was removed through column adsorption. The filtrate was collected,

concentrated by evaporation, and subsequently washed by methanol (3×). The resulting white precipitate was obtained by centrifugation and dried under vacuum to yield the macromonomer NB-P*n*BA-Br. ($M_{n,NMR}$ = 2,560 g mol^{-1} ; $M_{n,SEC}$ = 6,850 g mol^{-1}, M_n/M_w = 1.23). ^{1}H NMR ($CDCl_3$, δ, ppm): 6.15-5.93 (m, C***H***=C***H***), 4.03 (m, -OCOC***H₂***-), 1.59 (m, -OCOCH$_2$C***H₂***CH$_2$CH$_3$),1.35 (m, -OCOCH$_2$CH$_2$C***H₂***CH$_3$), 0.98 (t, -OCOCH$_2$CH$_2$CH$_2$C***H₃***).

4.4. Synthesis of the bottlebrush polymer of PNB-P*n*BA-Br. The bottlebrush polymer PNB-P*n*BA was synthesized via the ring-opening metathesis polymerization (ROMP) method.[21, 52] In a nitrogen atmosphere, macromonomer (PNB-P*n*BA-Br) (13.26 g, 1.93 mmol) was dissolved in 30 mL of DCM, resulting in a 25 wt% macromonomer concentration. Simultaneously, G_2 (15 mg, 0.018 mmol) was dissolved in 1 mL of DCM in a scintillation vial and then added to the above solution. The ROMP process was allowed to proceed at room temperature overnight. Finally, the product was precipitated in an excess amount of methanol and dried under vacuum to obtain the viscous bottlebrush polymer of PNB-P*n*BA-Br. ($M_{n,SEC}$ = 284,460 g mol^{-1}, M_n/M_w = 1.35). ^{1}H NMR ($CDCl_3$, δ, ppm): 4.03 (m, -OCOC***H₂***-), 1.59 (m, -OCOCH$_2$C***H₂***CH$_2$CH$_3$),1.35 (m, -OCOCH$_2$CH$_2$C***H₂***CH$_3$), 0.98 (t, -OCOCH$_2$CH$_2$CH$_2$C***H₃***).

4.5. Preparation of the Brush-DM. In a glass vial equipped with a stirring bar, 4.05 g of PNB-P*n*BA-Br (containing 1.6 mmol Br groups) (4.05 g, 1.6 mmol) was dissolved in dichloromethane (DCM) to form a solution with a mass fraction of 50 wt%. Subsequently, BDB (containing 1.2 mmol thiol groups) (0.20 g, 0.60 mmol) serving as the crosslinker, LiTSFI (0.80 g, 2.78 mmol), and two drops of TEA, acting as the catalyst, were added to the mixture. To achieve desired shapes for the elastomers, the solution was poured into a PTFE mold. The substitution reaction between the amino group and the bromine on the side chain of the

bottlebrush polymer, PNB-P*n*BA-Br, was allowed to proceed for 24 hours at an elevated temperature of 50 ℃. Following the reaction, the excess solvent was removed under vacuum to obtain the target elastomer. Furthermore, the preparation of Brush-NM utilized 1,6-hexanedithiol as the crosslinker with a dosage of 0.1 g (at the same molar concentration), following the same procedures as in the preparation of Brush-DM.

ASSOCIATED CONTENT

Supporting Information

The Supporting Information is available free of charge at https://pubs.acs.org/doi/10.1021/xxx. Characterizations, synthesis of BDB, preparation of Linear-NM, and assemble of the Brush-DM based flexible sensor. Table S1: Summary of the interfacial toughness of different materials. Scheme S1-S2: Synthetic route of BDB, and Linear-NM. Figure S1-S12: FT-IR and ^{1}H NMR spectrum of BDB; environmental stability of Brush-DM; Strain-sweeping measurement of Brush-DM; Relaxation behavior of prepared samples; Cyclic mechanical performance of Brush-DM; Relative resistance variations of the Brush-DM-based and Linear-NM-based sensors; Electronic pattern of the Brush-DM-based sensor during cyclic loading-unloading process; Relative resistance variations of the sensor in different stored time at 90% RH and 50 ℃ with 100% maximum strain; Electronic patterns of the flexible sensor during the cyclic finger bending.

AUTHOR INFORMATION

Corresponding Author

Email: xhyu@mail.dhu.edu.cn
Email: xsfan@dhu.edu.cn

Author Contributions

The manuscript was written through contributions of all authors. All authors have given approval to the final version of the manuscript.

Notes

The authors declare no competing financial interest.

ACKNOWLEDGMENT

X. Yu would like to acknowledge the financially supported from the Agency for Science, Technology and Research (A*STAR) under its RIE2025 Manufacturing, Trade and Connectivity (MTC) Programmatic Funding (Grant No. M22K9b0049). This work was financially supported by the National Natural Science Foundation of China (Grant No. U1504214).

REFERENCES

1. Han, S.-T.; Peng, H.; Sun, Q.; Venkatesh, S.; Chung, K.-S.; Lau, S. C.; Zhou, Y.; Roy, V. A. L., An Overview of the Development of Flexible Sensors. *Advanced Materials* **2017,** *29* (33), 1700375.
2. Rim, Y. S.; Bae, S.-H.; Chen, H.; De Marco, N.; Yang, Y., Recent Progress in Materials and Devices toward Printable and Flexible Sensors. *Advanced Materials* **2016,** *28* (22), 4415-4440.
3. Wang, Z.; Wei, H.; Huang, Y.; Wei, Y.; Chen, J., Naturally sourced hydrogels: emerging fundamental materials for next-generation healthcare sensing. *Chemical Society Reviews* **2023,** *52* (9), 2992-3034.
4. Senthil Kumar, K.; Chen, P.-Y.; Ren, H., A Review of Printable Flexible and Stretchable Tactile Sensors. *Research 2019*.
5. Jang, H.; Park, Y. J.; Chen, X.; Das, T.; Kim, M.-S.; Ahn, J.-H., Graphene-Based Flexible and Stretchable Electronics. *Advanced Materials* **2016,** *28* (22), 4184-4202.
6. Liu, S.; Zheng, R.; Chen, S.; Wu, Y.; Liu, H.; Wang, P.; Deng, Z.; Liu, L., A compliant, self-adhesive and self-healing wearable hydrogel as epidermal strain sensor. *Journal of Materials Chemistry C* **2018,** *6* (15), 4183-4190.
7. Reynolds, V. G.; Mukherjee, S.; Xie, R.; Levi, A. E.; Atassi, A.; Uchiyama, T.; Wang, H.; Chabinyc, M. L.; Bates, C. M., Super-soft solvent-free bottlebrush elastomers for

touch sensing. *Materials Horizons* **2020,** *7* (1), 181-187.
8. Yu, X.; Zhang, H.; Wang, Y.; Fan, X.; Li, Z.; Zhang, X.; Liu, T., Highly Stretchable, Ultra-Soft, and Fast Self-Healable Conductive Hydrogels Based on Polyaniline Nanoparticles for Sensitive Flexible Sensors. *Advanced Functional Materials* **2022,** *32* (33), 2204366.
9. Lee, Y.; Myoung, J.; Cho, S.; Park, J.; Kim, J.; Lee, H.; Lee, Y.; Lee, S.; Baig, C.; Ko, H., Bioinspired Gradient Conductivity and Stiffness for Ultrasensitive Electronic Skins. *ACS Nano* **2021,** *15* (1), 1795-1804.
10. Bian, G.; Pan, N.; Luan, Z.; Sui, X.; Fan, W.; Xia, Y.; Sui, K.; Jiang, L., Anti-Swelling Gradient Polyelectrolyte Hydrogel Membranes as High-Performance Osmotic Energy Generators. *Angewandte Chemie International Edition* **2021,** *60* (37), 20294-20300.
11. Gao, Y.; Jia, F.; Gao, G., Ultra-thin, transparent, anti-freezing organohydrogel film responded to a wide range of humidity and temperature. *Chemical Engineering Journal* **2022,** *430*, 132919.
12. Boland, C. S.; Khan, U.; Ryan, G.; Barwich, S.; Charifou, R.; Harvey, A.; Backes, C.; Li, Z.; Ferreira, M. S.; Möbius, M. E.; Young, R. J.; Coleman, J. N., Sensitive electromechanical sensors using viscoelastic graphene-polymer nanocomposites. *Science* **2016,** *354* (6317), 1257-1260.
13. Chen, F.; Gu, Y.; Cao, S.; Li, Y.; Li, F.; Zhang, X.; Xu, M.; Zhang, Y., Low-cost highly sensitive strain sensors for wearable electronics. *Journal of Materials Chemistry C* **2017,** *5* (40), 10571-10577.
14. Zhu, T.; Ni, Y.; Biesold, G. M.; Cheng, Y.; Ge, M.; Li, H.; Huang, J.; Lin, Z.; Lai, Y., Recent advances in conductive hydrogels: classifications, properties, and applications. *Chemical Society Reviews* **2023,** *52* (2), 473-509.
15. Liu, X.; Liu, J.; Lin, S.; Zhao, X., Hydrogel machines. *Materials Today* **2020,** *36*, 102-124.
16. Zhang, X.; Cui, C.; Chen, S.; Meng, L.; Zhao, H.; Xu, F.; Yang, J., Adhesive Ionohydrogels Based on Ionic Liquid/Water Binary Solvents with Freezing Tolerance for Flexible Ionotronic Devices. *Chemistry of Materials* **2022,** *34* (3), 1065-1077.
17. Yu, X.; Wang, Y.; Zhang, H.; Fan, X.; Liu, T., Ultrastretchable and Stable Conductive Elastomer Based on Micro-Ionicgel for Wide-Working-Range Sensors. *ACS Applied Materials & Interfaces* **2021,** *13* (44), 53091-53098.
18. Song, H.; Sun, Y.; Zhu, J.; Xu, J.; Zhang, C.; Liu, T., Hydrogen-bonded network enables polyelectrolyte complex hydrogels with high stretchability, excellent fatigue resistance and self-healability for human motion detection. *Composites Part B: Engineering* **2021,** *217*, 108901.
19. Yu, X.; Zheng, Y.; Wang, Y.; Zhang, H.; Song, H.; Li, Z.; Fan, X.; Liu, T., Facile Fabrication of Highly Stretchable, Stable, and Self-Healing Ion-Conductive Sensors for Monitoring Human Motions. *Chemistry of Materials* **2022,** *34* (3), 1110-1120.
20. Pakula, T.; Zhang, Y.; Matyjaszewski, K.; Lee, H.-i.; Boerner, H.; Qin, S.; Berry, G. C., Molecular brushes as super-soft elastomers. *Polymer* **2006,** *47* (20), 7198-7206.
21. Yu, X.; Wang, Y.; Li, M.; Zhang, Y.; Huang, Y.; Qian, Q.; Zheng, Y.; Hou, Q.; Fan, X., Self-Healable, Stretchable, and Super-Soft Bottlebrush Polyester Elastomers for Highly Sensitive Flexible Sensors. *ACS Applied Polymer Materials* **2023,** *5* (4), 2750-2759.

22. Que, Y.; Liu, Y.; Tan, W.; Feng, C.; Shi, P.; Li, Y.; Xiaoyu, H., Enhancing Photodynamic Therapy Efficacy by Using Fluorinated Nanoplatform. *ACS Macro Letters* **2016,** *5* (2), 168-173.
23. Xu, B.; Feng, C.; Hu, J.; Shi, P.; Gu, G.; Wang, L.; Huang, X., Spin-Casting Polymer Brush Films for Stimuli-Responsive and Anti-Fouling Surfaces. *ACS Applied Materials & Interfaces* **2016,** *8* (10), 6685-6692.
24. Tao, D.; Feng, C.; Cui, Y.; Yang, X.; Manners, I.; Winnik, M. A.; Huang, X., Monodisperse Fiber-like Micelles of Controlled Length and Composition with an Oligo(p-phenylenevinylene) Core via "Living" Crystallization-Driven Self-Assembly. *Journal of the American Chemical Society* **2017,** *139* (21), 7136-7139.
25. Xu, B.; Feng, C.; Huang, X., A versatile platform for precise synthesis of asymmetric molecular brush in one shot. *Nature Communications* **2017,** *8* (1), 333.
26. Xu, B.; Liu, Y.; Sun, X.; Hu, J.; Shi, P.; Huang, X., Semifluorinated Synergistic Nonfouling/Fouling-Release Surface. *ACS Applied Materials & Interfaces* **2017,** *9* (19), 16517-16523.
27. Feng, C.; Huang, X., Polymer Brushes: Efficient Synthesis and Applications. *Accounts of Chemical Research* **2018,** *51* (9), 2314-2323.
28. Sarapas, J. M.; Chan, E. P.; Rettner, E. M.; Beers, K. L., Compressing and Swelling To Study the Structure of Extremely Soft Bottlebrush Networks Prepared by ROMP. *Macromolecules* **2018,** *51* (6), 2359-2366.
29. Kim, N.-Y.; Moon, J.; Ryou, M.-H.; Kim, S.-H.; Kim, J.-H.; Kim, J.-M.; Bang, J.; Lee, S.-Y., Amphiphilic Bottlebrush Polymeric Binders for High-Mass-Loading Cathodes in Lithium-Ion Batteries. *Advanced Energy Materials* **2022,** *12* (1), 2102109.
30. Tao, D.; Wang, Z.; Huang, X.; Tian, M.; Lu, G.; Manners, I.; Winnik, M. A.; Feng, C., Continuous and Segmented Semiconducting Fiber-like Nanostructures with Spatially Selective Functionalization by Living Crystallization-Driven Self-Assembly. *Angewandte Chemie International Edition* **2020,** *59* (21), 8232-8239.
31. Xu, B.; Feng, C.; Lv, Y.; Lin, S.; Lu, G.; Huang, X., Biomimetic Asymmetric Polymer Brush Coatings Bearing Fencelike Conformation Exhibit Superior Protection and Antifouling Performance. *ACS Applied Materials & Interfaces* **2020,** *12* (1), 1588-1596.
32. Wang, S.; Zhang, S.; Feng, C.; Lu, G.; Theato, P.; Huang, X., Modification of polybutadiene with trifluoromethyl and clickable azide groups in one shot. *Polymer Chemistry* **2021,** *12* (39), 5589-5597.
33. Chen, R.; Jiang, X.; Lu, G.; Liu, W.; Jin, W.; Tian, G.; Huang, X., A well-defined thermo- and pH-responsive double hydrophilic graft copolymer bearing pyridine-containing backbone. *Polymer Chemistry* **2022,** *13* (19), 2791-2802.
34. Nie, F.-M.; An, C.-H.; Cao, D.-F.; Liu, J.; Zhou, Y.-F.; Lu, Y.-G.; Ma, Z.; Pan, L.; Li, Y.-S., Ru(II) Catalyst Enables Dynamic Dual-Cross-Linked Elastomers with Near-Infrared Self-Healing toward Flexible Electronics. *Advanced Functional Materials* **2022,** *32* (15), 2110616.
35. Zhou, M.; Liu, R.; Jia, D.; Cui, Y.; Liu, Q.; Liu, S.; Wu, D., Ultrathin Yet Robust Single Lithium-Ion Conducting Quasi-Solid-State Polymer-Brush Electrolytes Enable Ultralong-Life and Dendrite-Free Lithium-Metal Batteries. *Advanced Materials* **2021,** *33* (29), 2100943.

36. Cho, S.; Hwang, S. Y.; Oh, D. X.; Park, J., Recent progress in self-healing polymers and hydrogels based on reversible dynamic B–O bonds: boronic/boronate esters, borax, and benzoxaborole. *Journal of Materials Chemistry A* **2021,** *9* (26), 14630-14655.
37. Luo, J.; Demchuk, Z.; Zhao, X.; Saito, T.; Tian, M.; Sokolov, A. P.; Cao, P.-F., Elastic vitrimers: Beyond thermoplastic and thermoset elastomers. *Matter* **2022,** *5* (5), 1391-1422.
38. Ganewatta, M. S.; Wang, Z.; Tang, C., Chemical syntheses of bioinspired and biomimetic polymers toward biobased materials. *Nature Reviews Chemistry* **2021,** *5* (11), 753-772.
39. Aida, T.; Meijer, E. W.; Stupp, S. I., Functional Supramolecular Polymers. *Science* **2012,** *335* (6070), 813-817.
40. Jia, F.; Song, J.; Kubiak, J. M.; Onoda, M.; Santos, P. J.; Sano, K.; Holten-Andersen, N.; Zhang, K.; Macfarlane, R. J., Brush Polymers as Nanoscale Building Blocks for Hydrogel Synthesis. *Chemistry of Materials* **2021,** *33* (14), 5748-5756.
41. Shan, S.; Wu, X.; Lin, Y.; Zhang, A., Tough, Self-Healing, Recyclable Bottlebrush Polyurethane Elastomer with a Skin-like Strain-Adaptive-Strengthening Property. *ACS Applied Polymer Materials* **2022,** *4* (10), 7554-7563.
42. Xie, R.; Lapkriengkri, I.; Pramanik, N. B.; Mukherjee, S.; Blankenship, J. R.; Albanese, K.; Wang, H.; Chabinyc, M. L.; Bates, C. M., Hydrogen-Bonding Bottlebrush Networks: Self-Healing Materials from Super-Soft to Stiff. *Macromolecules* **2022,** *55* (23), 10513-10521.
43. Yu, X.; Zheng, Y.; Zhang, H.; Wang, Y.; Fan, X.; Liu, T., Fast-Recoverable, Self-Healable, and Adhesive Nanocomposite Hydrogel Consisting of Hybrid Nanoparticles for Ultrasensitive Strain and Pressure Sensing. *Chemistry of Materials* **2021,** *33* (15), 6146-6157.
44. Huang, Y.; Zhu, T.; Zhu, Z.; Yuan, H.; Tan, L.; Yao, P.; Qiao, Y.; Zhu, C.; Xu, J., Mussel-Inspired Adhesive and Carbon Fiber Conductive Hydrogel for Flexible Sensors. *ACS Applied Polymer Materials* **2023,** *5* (7), 5707-5715.
45. Mao, J.; Zhao, C.; Liu, L.; Li, Y.; Xiang, D.; Wu, Y.; Li, H., Adhesive, transparent, stretchable, and strain-sensitive hydrogel as flexible strain sensor. *Composites Communications* **2021,** *25*, 100733.
46. Zhao, H.; Hao, S.; Fu, Q.; Zhang, X.; Meng, L.; Xu, F.; Yang, J., Ultrafast Fabrication of Lignin-Encapsulated Silica Nanoparticles Reinforced Conductive Hydrogels with High Elasticity and Self-Adhesion for Strain Sensors. *Chemistry of Materials* **2022,** *34* (11), 5258-5272.
47. Nam, S.; Mooney, D., Polymeric Tissue Adhesives. *Chemical Reviews* **2021,** *121* (18), 11336-11384.
48. Shim, H. J.; Sunwoo, S.-H.; Kim, Y.; Koo, J. H.; Kim, D.-H., Functionalized Elastomers for Intrinsically Soft and Biointegrated Electronics. *Advanced Healthcare Materials* **2021,** *10* (17), 2002105.
49. Beyer, V. P.; Cattoz, B.; Strong, A.; Phillips, D. J.; Schwarz, A.; Remzi Becer, C., Fast track access to multi-block copolymers via thiol-bromo click reaction of telechelic dibromo polymers. *Polymer Chemistry* **2019,** *10* (31), 4259-4270.
50. Xiong, H.; Zhang, L.; Wu, Q.; Zhang, H.; Peng, Y.; Zhao, L.; Huang, G.; Wu, J., A strain-adaptive, self-healing, breathable and perceptive bottle-brush material inspired by

skin. *Journal of Materials Chemistry A* **2020,** *8* (46), 24645-24654.
51. Li, S.; Jiang, K.; Wang, J.; Zuo, C.; Jo, Y. H.; He, D.; Xie, X.; Xue, Z., Molecular Brush with Dense PEG Side Chains: Design of a Well-Defined Polymer Electrolyte for Lithium-Ion Batteries. *Macromolecules* **2019,** *52* (19), 7234-7243.
52. Miao, W.; Yang, B.; Jin, B.; Ni, C.; Feng, H.; Xue, Y.; Zheng, N.; Zhao, Q.; Shen, Y.; Xie, T., An Orthogonal Dynamic Covalent Polymer Network with Distinctive Topology Transformations for Shape- and Molecular Architecture Reconfiguration. *Angewandte Chemie International Edition* **2022,** *61* (11), e202109941.
53. Huang, Q.; Tang, Z.; Wang, D.; Wu, S.; Guo, B., Engineering Segregated Structures in a Cross-Linked Elastomeric Network Enabled by Dynamic Cross-Link Reshuffling. *ACS Macro Letters* **2021,** *10* (2), 231-236.
54. Wang, Y.; Yu, X.; Zhang, H.; Fan, X.; Zhang, Y.; Li, Z.; Miao, Y.-E.; Zhang, X.; Liu, T., Highly Stretchable, Soft, Low-Hysteresis, and Self-Healable Ionic Conductive Elastomers Enabled by Long, Functional Cross-Linkers. *Macromolecules* **2022,** *55* (17), 7845-7855.
55. Beyer, V. P.; Cattoz, B.; Becer, C. R., Thiol-Bromo Click Reaction for One-Pot Synthesis of Star-Shaped Polymers. *Macromolecular Rapid Communications* **2021,** *42* (2), 2000519.
56. Shi, L.; Zhu, T.; Gao, G.; Zhang, X.; Wei, W.; Liu, W.; Ding, S., Highly stretchable and transparent ionic conducting elastomers. *Nature Communications* **2018,** *9* (1), 2630.
57. Lee, M. J.; Han, J.; Lee, K.; Lee, Y. J.; Kim, B. G.; Jung, K.-N.; Kim, B. J.; Lee, S. W., Elastomeric electrolytes for high-energy solid-state lithium batteries. *Nature* **2022,** *601* (7892), 217-222.
58. Xu, K.; Wang, Y.; Zhang, B.; Zhang, C.; Liu, T., Stretchable and self-healing polyvinyl alcohol/cellulose nanofiber nanocomposite hydrogels for strain sensors with high sensitivity and linearity. *Composites Communications* **2021,** *24*, 100677.
59. Mei, H.; Mah, A. H.; Hu, Z.; Li, Y.; Terlier, T.; Stein, G. E.; Verduzco, R., Rapid Processing of Bottlebrush Coatings through UV-Induced Cross-Linking. *ACS Macro Letters* **2020,** *9* (8), 1135-1142.
60. Cromwell, O. R.; Chung, J.; Guan, Z., Malleable and Self-Healing Covalent Polymer Networks through Tunable Dynamic Boronic Ester Bonds. *Journal of the American Chemical Society* **2015,** *137* (20), 6492-6495.
61. Röttger, M.; Domenech, T.; van der Weegen, R.; Breuillac, A.; Nicolaÿ, R.; Leibler, L., High-performance vitrimers from commodity thermoplastics through dioxaborolane metathesis. *Science* **2017,** *356* (6333), 62-65.
62. Wiener, C. G.; Wang, C.; Liu, Y.; Weiss, R. A.; Vogt, B. D., Nanostructure Evolution during Relaxation from a Large Step Strain in a Supramolecular Copolymer-Based Hydrogel: A SANS Investigation. *Macromolecules* **2017,** *50* (4), 1672-1680.
63. Kuang, X.; Liu, G.; Dong, X.; Wang, D., Correlation between stress relaxation dynamics and thermochemistry for covalent adaptive networks polymers. *Materials Chemistry Frontiers* **2017,** *1* (1), 111-118.
64. Miao, W.; Zou, W.; Luo, Y.; Zheng, N.; Zhao, Q.; Xie, T., Structural tuning of polycaprolactone based thermadapt shape memory polymer. *Polymer Chemistry* **2020,** *11* (7), 1369-1374.

65. Maw, M. R.; Tanas, A. K.; Dashtimoghadam, E.; Nikitina, E. A.; Ivanov, D. A.; Dobrynin, A. V.; Vatankhah-Varnosfaderani, M.; Sheiko, S. S., Bottlebrush Thermoplastic Elastomers as Hot-Melt Pressure-Sensitive Adhesives. *ACS Applied Materials & Interfaces* **2023,** *15* (35), 41870-41879.
66. Tan, Y.; Chen, H.; Kang, W.; Wang, X., Versatile Light-Mediated Synthesis of Dry Ion-Conducting Dynamic Bottlebrush Networks with High Elasticity, Interfacial Adhesiveness, and Flame Retardancy. *Macromolecules* **2022,** *55* (21), 9715-9725.
67. Zhou, C.; Xu, S.; Pi, P.; Cheng, J.; Wang, L.; Yang, J.; Wen, X., Polyacrylate/silica nanoparticles hybrid emulsion coating with high silica content for high hardness and dry-wear-resistant. *Progress in Organic Coatings* **2018,** *121*, 30-37.
68. Song, H.; Yu, X.; Nguyen, D. H.; Zhang, C.; Liu, T., Highly stretchable, self-healable and self-adhesive polyzwitterion ionogels enabled with binary noncovalent interactions. *Composites Communications* **2022,** *34*, 101251.
69. Arrington, K. J.; Radzinski, S. C.; Drummey, K. J.; Long, T. E.; Matson, J. B., Reversibly Cross-linkable Bottlebrush Polymers as Pressure-Sensitive Adhesives. *ACS Applied Materials & Interfaces* **2018,** *10* (31), 26662-26668.
70. Yuk, H.; Zhang, T.; Parada, G. A.; Liu, X.; Zhao, X., Skin-inspired hydrogel–elastomer hybrids with robust interfaces and functional microstructures. *Nature Communications* **2016,** *7* (1), 12028.